PHYSICAL REVIEW B **89**, 195205 (2014)

Electrostatics-based finite-size corrections for first-principles point defect calculations

Yu Kumagai[1,*] and Fumiyasu Oba[1,2]

[1]*Materials Research Center for Element Strategy, Tokyo Institute of Technology, Yokohama 226-8503, Japan*

[2]*Department of Materials Science and Engineering, Kyoto University, Kyoto 606-8501, Japan*

(Received 9 February 2014; revised manuscript received 22 April 2014; published 23 May 2014)

Finite-size corrections for charged defect supercell calculations typically consist of image-charge and potential alignment corrections. Regarding the image-charge correction, Freysoldt, Neugebauer, and Van de Walle (FNV) recently proposed a scheme that constructs the correction energy *a posteriori* through alignment of the defect-induced potential to a model charge potential [C. Freysoldt *et al.*, Phys. Rev. Lett. **102**, 016402 (2009)]. This, however, still has two shortcomings in practice. First, it uses a planar-averaged electrostatic potential for determining the potential offset, which can not be readily applied to defects with large atomic relaxation. Second, Coulomb interaction is screened by a macroscopic scalar dielectric constant, which can bring forth large errors for defects in layered and low-dimensional structures. In this study, we use the atomic site potential as a potential marker, and extend the FNV scheme by estimating long-range Coulomb interactions with a point charge model in an anisotropic medium. We also revisit the conventional potential alignment and show that it is unnecessary for correcting defect formation energies after the image-charge correction is properly applied. A systematic assessment of the accuracy of the extended FNV scheme is performed for defects and impurities in diverse materials: β-Li_2TiO_3, ZnO, MgO, Al_2O_3, HfO_2, cubic and hexagonal BN, Si, GaAs, and diamond. Defect formation energies with -6 to $+3$ charges calculated using supercells containing around 100 atoms are successfully corrected even after atomic relaxation within 0.2 eV compared to those in the dilute limit.

DOI: 10.1103/PhysRevB.89.195205 PACS number(s): 61.72.J−, 71.15.Mb, 71.55.−i

I. INTRODUCTION: CORRECTION SCHEMES ON FIRST-PRINCIPLES POINT DEFECT CALCULATIONS

Point defects and impurities are ubiquitous in semiconductors or insulators and strongly dominate a wide variety of material properties such as optical, mechanical, electrical, and transport properties, having a decisive impact on their performance in applications, e.g., photovoltaics, photocatalysts, ionic conductors, transistors, and light-emitting diodes. Therefore, knowledge and precise control of defects are inherently the key to the smart design of materials with superior performance. Despite the importance, it is difficult to directly and fully study point defects by experiments, and first-principles calculations have emerged as an invaluable tool for modeling and understanding point defects in particular thanks to rapid progress on the computational speed and electronic-structure calculation methods [1–4]. These calculations support and complement experimental findings.

First-principles point defect calculations commonly rely on the supercell approach under the periodic boundary condition. However, the cell sizes are not usually sufficiently large for describing the low concentration of defects in realistic materials such as 10^{14}–10^{18} cm^{-3}. Calculations using common approximations to density functional theory (DFT), viz. local density approximation (LDA) or generalized gradient approximation (GGA), can treat a few thousand atoms at most, and hybrid functionals such as the Heyd-Scuseria-Ernzerhof functional (HSE06) [5,6] up to a few hundred atoms, which corresponds to 10^{20}–10^{21} cm^{-3}. Formation energies of the charged defects calculated with such small supercells could include huge convergence errors up to several eV, especially for highly charged defects. In the case that the defect charge is fully contained in the supercell, the main source of the error comes from the spurious long-range Coulomb interactions between the defect charge, its periodic images, and background charge [7,8], the last of which is required for avoiding the divergence of the electrostatic energy. Consequently, the formation energy slowly converges with the supercell size. A correction for removing the spurious interactions, which we call the image-charge correction, is therefore valuable for precisely evaluating the defect formation energy in the isolated limit unless the dielectric constant is large enough to screen the interactions. In addition, since the average electrostatic potential in the entire supercell is conventionally set to zero by removing a constant in the Fourier transformation of electrostatic potential, the eigenvalues are defined only up to an undetermined constant [9]. Whereas the total energies of charge-neutral systems, including both molecular systems in vacuum and defective systems in crystals, are well defined, those of charged systems depend on this arbitrary shift of the electrostatic potential. Therefore, it has been believed that one needs to align the valence band maximum (VBM) in the calculation of a charged defect to that of the pristine host for restoring physically meaningful formation energies [2,10]. We define the alignment of the VBM as potential alignment in this study.

A number of image-charge correction schemes have been devised since a few decades ago [7,11–18]. The simplest correction is the point charge (PC) correction, which is the leading term for correcting spurious electrostatic interactions. Usually, the PC correction energy is constructed with a scalar dielectric constant under the assumption that the dielectric response is isotropic. Recently, Rurali and Cartoixà derived the Ewald formalism for the more rigorous PC energy with a dielectric tensor and applied it to the Al substitution energy in one-dimensional Si nanowires [19], and later on Murphy and Hine applied it to the formation energies of the Ti vacancy

*yuuukuma@gmail.com

(V_{Ti}^{-4}), Li antisite on Ti (Li_{Ti}^{-3}), and oxygen interstitial (O_i^{-2}) in monoclinic β-Li_2TiO_3 [20]. Although the PC correction basically improves the defect formation energy, in some cases higher-order terms are not negligible, and the defect formation energy has to be extrapolated to the infinite interdefect distance limit with a set of supercell calculations. This is, however, prohibitive when a computational cost severely limits the size of supercells especially with hybrid functionals, quantum Monte Carlo, etc. [21–30].

Recently, Freysoldt, Neugebauer, and Van de Walle (FNV) proposed a scheme which allows us to correct the defect formation energies *a posteriori* through alignment of the defect-induced potential to a model charge potential [15,16]. The principal benefit of this scheme is to construct a correction energy from two supercell calculations with and without a defect. Therefore, it is useful especially when computationally expensive schemes are employed. We are, however, prevented from applying it to defects in practical applications by its two inherent shortcomings.

First, it uses a planar-averaged electrostatic potential to align the defect-induced potential obtained by subtracting the bulk supercell potential from the defective supercell potential to a model charge potential. This works well when the atomic positions are fixed in unrelaxed crystalline positions. However, accurate calculations require relaxation of atomic positions. As pointed out by Komsa *et al.* [8], the defect-induced potential strongly fluctuates when the atomic displacements are large even far from the defect in the supercell. Consequently, the potential offset between defect-induced potential and model charge potential has to be determined, e.g., by convoluting the defect-induced potential with a suitable Gaussian function [8]. Second, in the original paper, the long-range Coulomb interaction is calculated with a macroscopic scalar dielectric constant. This is acceptable when diagonal components of a dielectric tensor are close to each other and off-diagonal components are relatively small. To resolve these two practical deficiencies is necessary to expand the versatility of the scheme to broad classes of materials. Thus, we use atomic site electrostatic potential for evaluating the defect-induced potential and an anisotropic PC model for long-range Coulomb interactions. Since the FNV correction energy is the sum of the PC and alignmentlike correction energies as shown in Sec. III C, our extension can also be considered as an extension of the anisotropic PC correction scheme [19,20]. The FNV scheme in the anisotropic form is tested with layered compounds, hexagonal BN (h-BN) and β-Li_2TiO_3, as well as isotropic systems. Details are discussed in Secs. III and V.

There also exist a wide variety of ways to perform the potential alignment. In the most common approach, the potential is aligned so that the electrostatic potential at the outermost atomic sites in the supercell with a charged defect becomes the same as that of the bulk [2,31–33]. We call this conventional potential alignment in the following. Instead, Lany and Zunger adopted the reference by averaging potential differences from the perfect cell at all atomic sites except the immediate neighbors of a defect [10]. Taylor and Bruneval, however, demonstrated that the Madelung potential, which is taken into account by the first-order image-charge correction, brings a potential shift and one can not perform the image-charge correction and potential alignment independently [17]. In order to remove the long-range Coulomb interactions, Komsa *et al.* proposed a way to align the potential at the outermost area of the *neutral* defect to that of the pristine bulk [8]. Taylor and Bruneval also proposed to align the potential averaged over the entire supercell including exchange-correlation potential to the bulk potential [17]. In Sec. IV, we revisit the controversial potential alignment, and advocate that the potential alignment is unnecessary under the assumption that the image-charge correction is properly constructed.

The cell-size dependence of the FNV scheme for relaxed defects has been reported only by Komsa *et al.* with V_O^{+1} in MgO [8]. To assess the performance of the correction scheme is essential for practical applications. In Sec. V, we apply the extended FNV scheme introduced in this study to a wide variety of material classes: ZnO, MgO, corundum Al_2O_3, monoclinic HfO_2 (m-HfO_2), cubic BN (c-BN), Si, GaAs, and diamond in addition to β-Li_2TiO_3 and h-BN with layered structures and evaluate its accuracy for relaxed defects. In addition, we discuss the remaining error sources.

II. DETAILS OF FIRST-PRINCIPLES CALCULATIONS

We here summarize the details of the first-principles calculations used in this study. Our calculations were performed using the projector augmented-wave (PAW) method [34] as implemented in VASP [35,36]. We adopted Perdew-Burke-Ernzerhof GGA (PBE-GGA) [37] except for GaAs and diamond: The LDA [38] was used for GaAs because the band gap is more significantly underestimated with the PBE-GGA at the theoretical lattice constant (0.16 eV with the GGA versus 0.51 eV with the LDA), and the HSE06 hybrid functional for diamond in order to demonstrate how accurately the extended FNV scheme can correct HSE06 defect formation energies. A Hubbard U correction was applied to a Ce impurity in c-BN ($U - J = 4.5$ eV for f orbitals) [39,40].

In this study, Li 2s, B 2s and 2p, C 2s and 2p, N 2s and 2p, O 2s and 2p, Mg 3s, Al 3s and 3p, Si 3s and 3p, Ti 4s and 3d, Zn 4s and 3d, Ga 4s and 4p, As 4s and 4p, and Ce 4f, 5d, and 6s, and Hf 6s and 5d were described as valence electrons. The PAW data set with radial cutoffs of 1.08, 0.90, 0.70, 0.79, 0.80, 1.06, 1.01, 1.01, 1.48, 1.22, 1.38, 1.11, 1.36, and 1.59 Å was used for Li, B, C, N, O, Mg, Al, Si, Ti, Zn, Ga, As, Ce, and Hf, respectively. The average atomic site potential was evaluated within spheres of radii 0.97, 0.77, 0.79, 0.71, 0.72, 1.07, 1.04, 0.99, 1.28, 1.06, 1.26, 0.95, and 1.25 Å for Li, B, C, N, O, Mg, Al, Si, Ti, Zn, Ga, As, and Hf. Wave functions were expanded with plane waves up to energy cutoffs of 400 and 550 eV for the cases where lattice parameters were fixed and optimized, respectively. Integrations in reciprocal space for defect calculations were performed with k-point grids with $> 6.0 \times 10^3$ Å^3; the lowest k-point density is the Γ-point only sampling for a c-BN $5 \times 5 \times 5$ supercell. In this study, atomic positions were relaxed, whereas the lattice constants were fixed at the bulk optimized values for defect calculations. When analyzing the planar-averaged potential, the atomic positions were fixed in unrelaxed crystalline positions. Forces acting on the atoms and stresses were reduced to be less than 0.02 eV/Å and 0.1 GPa. The dielectric tensors are indispensable for the correction scheme of the defect formation energies discussed in this study. Both ion-clamped dielectric

TABLE I. Calculated lattice parameters in units of Å and degrees, ion-clamped (ε^{ele}) dielectric tensors and ionic contributions to the dielectric tensors (ε^{ion}) in ZnO (space group: $P6_3mc$), MgO ($Fm\bar{3}m$), Al_2O_3 ($R\bar{3}c$), HfO_2 ($P2_1/c$), c-BN ($F\bar{4}3m$), h-BN ($P6_3/mmc$), β-Li_2TiO_3 ($C2/c$), Si ($Fd3m$), GaAs ($F\bar{4}3m$), and diamond ($Fd3m$). Available experimental values are also shown. The experimental ε^{ele} are high-frequency dielectric constants ε^{∞}, and ε^{ion} are estimated by subtracting ε^{∞} from static dielectric constants. Note that ionic contributions of elemental substances (Si and diamond) are null because Born effective charges are zero.

	Lattice parameter	ε^{ele}	ε^{ion}
ZnO	$a = 3.29$ $b = 5.31$	$\varepsilon_\perp = 5.20$ $\varepsilon_\parallel = 5.22$	$\varepsilon_\perp = 5.14$ $\varepsilon_\parallel = 6.02$
Expt.[a]	$a = 3.250$ $b = 5.207$	$\varepsilon_\perp = 3.70$ $\varepsilon_\parallel = 3.78$	$\varepsilon_\perp = 4.07$ $\varepsilon_\parallel = 5.13$
MgO	$a = 4.25$	3.16	7.50
Expt.[b]	$a = 4.211$	3.0	6.6
Al_2O_3	$a = 4.81$ $c = 13.12$	$\varepsilon_\perp = 3.27$ $\varepsilon_\parallel = 3.24$	$\varepsilon_\perp = 6.74$ $\varepsilon_\parallel = 9.11$
Expt.[c]	$a = 4.76$ $c = 12.99$	$\varepsilon_\perp = 3.1$ $\varepsilon_\parallel = 3.1$	$\varepsilon_\perp = 6.3$ $\varepsilon_\parallel = 8.5$
HfO_2	$a = 5.14$ $b = 5.19$ $c = 5.32$ $\beta = 100$	$\varepsilon_{11} = 4.79$ $\varepsilon_{22} = 4.77$ $\varepsilon_{33} = 4.52$ $\varepsilon_{13} = -0.13$	$\varepsilon_{11} = 15.17$ $\varepsilon_{22} = 13.46$ $\varepsilon_{33} = 10.74$ $\varepsilon_{13} = -1.09$
Expt.[d]	$a = 5.117$ $b = 5.175$ $c = 5.292$ $\beta = 99$	NA	NA
β-Li_2TiO_3	$a = 5.09$ $b = 8.85$ $c = 9.82$ $\beta = 100$	$\varepsilon_{11} = 5.45$ $\varepsilon_{22} = 5.49$ $\varepsilon_{33} = 3.74$ $\varepsilon_{13} = 0.01$	$\varepsilon_{11} = 36.95$ $\varepsilon_{22} = 36.32$ $\varepsilon_{33} = 12.07$ $\varepsilon_{13} = -1.06$
Expt.[e]	$a = 5.06$ $b = 8.79$ $c = 9.75$ $\beta = 100$	NA	NA
c-BN	$a = 3.63$	4.61	2.34
Expt.[f]	$a = 3.616$	4.46	2.6
h-BN	$a = 2.51$[g] $c = 6.66$	$\varepsilon_\perp = 4.76$ $\varepsilon_\parallel = 2.68$	$\varepsilon_\perp = 1.83$ $\varepsilon_\parallel = 0.44$
Expt.[h]	$a = 2.5$ $c = 6.66$	$\varepsilon_\perp = 4.3$ $\varepsilon_\parallel = 2.2$	$\varepsilon_\perp = 2.6$ $\varepsilon_\parallel = 2.9$
Si	$a = 5.47$	12.98	
Expt.[i]	$a = 5.431$	11.7	
GaAs	$a = 5.63$	15.92	1.95
Expt.[j]	$a = 5.654$	11.1	2.0
diamond	$a = 3.55$	5.58	
Expt.[k]	$a = 3.567$	5.7	

[a]References [44,45].
[b]References [8,46].
[c]References [47,48].
[d]Reference [49].
[e]Reference [50].
[f]References [51,52].
[g]The lattice constant in the c direction is fixed to the experimental value.
[h]Reference [52].
[i]References [52,53].
[j]References [8,54].
[k]References [8,55].

tensors and ionic contributions to the dielectric tensors were calculated with density functional perturbation theory [41,42]. The ion-clamped electronic part includes local field effects within DFT. The ionic part was calculated with a finite different scheme [43].

The calculated lattice parameters and dielectric tensors are summarized in Table I. The lattice constants estimated with the PBE-GGA are systematically overestimated, a typical tendency in the PBE-GGA. The ion-clamped dielectric constants are overestimated compared to the experimental ones except for diamond that is treated using HSE06. This could be related to underestimation of the band gaps with the LDA and PBE-GGA. When the atomic positions are relaxed, dipoles of polarizable ions in addition to electrons screen the charged defects. Therefore, the sum of an ion-clamped dielectric tensor and an ionic contribution should be used for a relaxed system, whereas only an ion-clamped dielectric tensor is appropriate for an unrelaxed system [8].

III. IMAGE-CHARGE CORRECTION

The formation energy of defect D in charge state q can be written as [8,56]

$$E_f[D^q] = \{E[D^q] + E_{\rm corr}[D^q]\} - E_P - \sum_i n_i \mu_i + q\{(\varepsilon_{\rm VBM} + \Delta v) + \Delta\varepsilon_F\}. \quad (1)$$

Here, $E[D^q]$ and E_P are the total energies of the supercell with the defect D in charge state q and the perfect supercell without any defect, respectively. n_i is the number of removed ($n_i < 0$) or added ($n_i > 0$) i-type atoms and μ_i refers to the chemical potential. $\varepsilon_{\rm VBM}$ is the energy level of the VBM, and $\Delta\varepsilon_F$ is the Fermi level referenced to $\varepsilon_{\rm VBM}$. $E_{\rm corr}[D^q]$ and Δv, corresponding to the image-charge correction and potential alignment correction, respectively, are for charged defects. Then $\varepsilon_{\rm VBM} + \Delta v + \Delta\varepsilon_F$ ($= \varepsilon_F$) represents the Fermi level. We discuss relative defect formation energies as a function of cell size and corrections on them; thus, only $E[D^q] + E_{\rm corr}[D^q] - E_P + q\Delta v$ is meaningful in this study.

Here, we address ourselves to the image-charge correction schemes that have been devised over the last decades. The electrostatics-based image-charge correction is intended to subtract the spurious interaction energy caused by the defect image charges and background charge, and requires an assumption that the defect charge is localized in the supercell. Following Ref. [8], we consider three systems: (1) a pristine bulk system, (2) a system with a periodic array of localized defects with charge q and a neutralizing background charge with charge density $-\frac{q}{\Omega}$, where Ω is volume of the supercell, and (3) a system with a single isolated defect with charge q. The potential is represented with $V_{\rm bulk}$, $V_{{\rm defect},q}$, and $V_{{\rm isolated},q}$, respectively. Here and hereafter, to avoid confusions, we adopt the signs based on conventional electrostatic potential following Ref. [8]. The electron charge is then set to the negative value.

Another assumption is that charge density of a single defect within the supercell $\rho_d(\boldsymbol{r})$, which satisfies $q = \int_\Omega \rho_d(\boldsymbol{r})d\boldsymbol{r}$, is close to each other in periodic and isolated systems [13,57]. In other words, the variation of $\rho_d(\boldsymbol{r})$ induced by the spurious

potential caused by the periodic images and background charge is negligibly small. The electrostatic energy of a defect, its images, and background charge of the periodic system is

$$E_{\text{periodic}} = \frac{1}{2}\int_{\Omega}[V_{\text{defect},q}(\boldsymbol{r}) - V_{\text{bulk}}(\boldsymbol{r})]\left(\rho_d(\boldsymbol{r}) - \frac{q}{\Omega}\right)d\boldsymbol{r}. \tag{2}$$

The factor $\frac{1}{2}$ accounts for removing double counting, and the integration is performed over the supercell. We emphasize that Eq. (2) should in principle contain $-\frac{q}{\Omega}$ differing from Refs. [8,58]. The electrostatic energy of an isolated defect without the periodic boundary condition can be written as

$$E_{\text{isolated}} = \frac{1}{2}\int[V_{\text{isolated},q}(\boldsymbol{r}) - V_{\text{bulk}}(\boldsymbol{r})]\rho_d(\boldsymbol{r})d\boldsymbol{r}. \tag{3}$$

The integration is performed over *all space*. Following $\int_{\Omega} V_{\text{defect},q}d\boldsymbol{r} = 0$ and $\int_{\Omega} V_{\text{bulk}}d\boldsymbol{r} = 0$ by convention and the assumption that the defect charge is localized in the supercell, the correction on the defect formation energy is written as [8,58]

$$E_{\text{cor}} = E_{\text{isolated}} - E_{\text{periodic}} = \frac{1}{2}\int_{\Omega} V_{\text{cor}}(\boldsymbol{r})\rho_d(\boldsymbol{r})d\boldsymbol{r}, \tag{4}$$

where $V_{\text{cor}} = V_{\text{isolated},q} - V_{\text{defect},q}$. Note that the background charge density does not contribute to the correction energy due to the convention of zero-average potential.

A. Point-charge correction

The simplest image-charge correction is to subtract the PC energy. Only V_{cor} at the defect site is essential for the PC correction, and can be estimated by an Ewald summation. Fuchs derived the Ewald formalism for the Madelung energy of periodically repeating PCs immersed in a neutralizing background charge for the study of the stability of Cu metal [59]. Leslie and Gillan employed it for the corrections of defect formation energies [11]. Suppose that the long-range Coulomb interaction is screened by a scalar dielectric constant ε in an isotropic medium. The potential at defect site $\boldsymbol{R}_0$ caused by PCs with charge q located at periodic image sites $\boldsymbol{R}_i$ ($i \neq 0$) and the background charge with charge density $-\frac{q}{\Omega}$, namely Madelung potential, for a cubic cell is [59]

$$V^{\text{iso}}_{\text{PC},q} = -\frac{\alpha q}{\varepsilon L} = \frac{q}{\varepsilon}\left\{\sum_{\boldsymbol{R}_i}^{i\neq 0}\frac{\text{erfc}(\gamma|\boldsymbol{R}_i|)}{|\boldsymbol{R}_i|} - \frac{\pi}{\Omega\gamma^2} + \sum_{\boldsymbol{G}_i}^{i\neq 0}\frac{4\pi}{\Omega}\frac{\exp(-\boldsymbol{G}_i{}^2/4\gamma^2)}{\boldsymbol{G}_i{}^2} - \frac{2\gamma}{\sqrt{\pi}}\right\}, \tag{5}$$

where the summations of $\boldsymbol{R}_i$ and $\boldsymbol{G}_i$ run over all vectors of the direct and reciprocal lattices except $\boldsymbol{R}_0$ and $\boldsymbol{G}_0 = \boldsymbol{0}$, and L is the dimension of the supercell, α the Madelung constant which depends on the Bravais lattice, and γ a suitably chosen convergence parameter which does not affect the potential [11,59]. Here and hereafter, we suppose that a single defect exists in the supercell, and its coordinate is taken to be $\boldsymbol{r} = \boldsymbol{R}_0 = \boldsymbol{0}$. Note that the second term, which is absent in the charge-neutral Ewald summation without the background charge, is essential for correcting the potential shift introduced by a periodic array of Gaussian charges instead of PCs in the third term [59], and obtained by

$$-\frac{1}{\Omega}\int_0^{\infty}\frac{\text{erfc}(\gamma r)}{r}4\pi r^2 dr = -\frac{\pi}{\Omega\gamma^2}. \tag{6}$$

The fourth term corresponds to the cancellation of the potential introduced by the Gaussian located at $\boldsymbol{r} = \boldsymbol{0}$ which is included in the third term. The correction potential is then $V_{\text{cor}} = -V^{\text{iso}}_{\text{PC},q}$. This is the same as the functional derivative of the PC correction energy with respect to the defect charge density [8,17]. The PC correction energy is then written as

$$E^{\text{iso}}_{\text{PC}} = \frac{1}{2}\int_{\Omega}\left(-V^{\text{iso}}_{\text{PC},q}\right)q\delta(\boldsymbol{r})d\boldsymbol{r} = -\frac{q}{2}V^{\text{iso}}_{\text{PC},q} = \frac{\alpha q^2}{2\varepsilon L}. \tag{7}$$

The use of a dielectric constant is valid for systems with nearly isotropic dielectric response, and it should be replaced by a dielectric tensor $\bar{\varepsilon}$ for the others, especially layered and low-dimensional materials [20]. With the principal axis transformation in conjunction with Eq. (5) [60], Rurali and Cartoixà derived the Ewald formalism for the Madelung potential with $\bar{\varepsilon}$ as

$$V^{\text{aniso}}_{\text{PC},q} = \sum_{\boldsymbol{R}_i}^{i\neq 0}\frac{q}{\sqrt{|\bar{\varepsilon}|}}\frac{\text{erfc}(\gamma\sqrt{\boldsymbol{R}_i\cdot\bar{\varepsilon}^{-1}\cdot\boldsymbol{R}_i})}{\sqrt{\boldsymbol{R}_i\cdot\bar{\varepsilon}^{-1}\cdot\boldsymbol{R}_i}} - \frac{\pi q}{\Omega\gamma^2} + \sum_{\boldsymbol{G}_i}^{i\neq 0}\frac{4\pi q}{\Omega}\frac{\exp(-\boldsymbol{G}_i\cdot\bar{\varepsilon}\cdot\boldsymbol{G}_i/4\gamma^2)}{\boldsymbol{G}_i\cdot\bar{\varepsilon}\cdot\boldsymbol{G}_i} - \frac{2\gamma q}{\sqrt{\pi\,|\bar{\varepsilon}|}}. \tag{8}$$

When the normalized coordinates are changed to regular Cartesian coordinates, Ω changes to $\Omega/\sqrt{|\bar{\varepsilon}|}$ [60]. This cancels out $\sqrt{|\bar{\varepsilon}|}$ in the second and third terms. The correction energy is then written as $E^{\text{aniso}}_{\text{PC}} = -\frac{q}{2}V^{\text{aniso}}_{\text{PC},q}$. Murphy and Hine applied it to correct the defect formation energies in monoclinic β-Li_2TiO_3 and showed the importance of the anisotropic extension [20]. Very recently, Petretto and Bruneval also corrected the energies of the Zn vacancy, group-V dopants, and their complexes in ZnO with it [61].

B. Makov-Payne correction

The PC correction is the leading term of the image-charge correction with the L^{-1} order. Makov and Payne (MP) then derived the correction term with the L^{-3} order [12]. Dabo *et al.* later rederived the same formula in a simpler and physically intuitive manner [58]. Following Refs. [12,58], the correction potential V_{cor} for a defect in a periodically repeated cubic cell is written as

$$V^{\text{iso}}_{\text{MP}}(\boldsymbol{r}) = -V^{\text{iso}}_{\text{PC,q}} - \frac{2\pi q}{3\varepsilon L^3}r^2 + \frac{4\pi}{3\varepsilon L^3}\boldsymbol{p}\cdot\boldsymbol{r} - \frac{2\pi Q}{3\varepsilon L^3} + O(r^4). \tag{9}$$

Here, $\boldsymbol{p} = \int\boldsymbol{r}\rho_d(\boldsymbol{r})d\boldsymbol{r}$ is the dipole moment and $Q = \int r^2\rho_d(\boldsymbol{r})d\boldsymbol{r}$ the second radial moment. The correction energy under the cubic symmetry up to the L^{-3} order is then

$$E^{\text{iso}}_{\text{MP}} = \frac{1}{2}\int_{\Omega}V^{\text{iso}}_{\text{MP}}(\boldsymbol{r})\rho_d(\boldsymbol{r})d\boldsymbol{r} = E^{\text{iso}}_{\text{PC}} - \frac{2\pi qQ}{3\varepsilon L^3} + \frac{2\pi\boldsymbol{p}^2}{3\varepsilon L^3} + O(L^{-5}). \tag{10}$$

Assuming that the dipole moment is negligible, the third term can be omitted. For charged ions and molecules in vacuum under the periodic boundary condition, we can exactly calculate $E_{\rm MP}^{\rm iso}$ up to the third order as discussed in Sec. IV. However, there are some difficulties for defects in crystalline materials. First, the defect charge ρ_d is ill defined because the immersed ρ_d and screening charge are inseparable; thus, Q can not be calculated directly [7,8]. Second, the Coulomb interaction can be assumed to be screened by a scalar dielectric constant, which is suited only for systems with nearly isotropic dielectric response. It is also doubtful that the short-range Coulomb interaction can be assumed to be screened by the scalar dielectric constant. Therefore, $E_{\rm MP}^{\rm iso}$ is usually not directly evaluated and estimated by fitting the energies calculated with various supercells with different sizes and shapes [14,18,24]. Such calculations need massive computational resource especially for large supercells and are not accessible with advanced DFT and many-body theory calculations.

C. FNV correction

Later on, Freysoldt, Neugebauer, and Van de Walle proposed another correction scheme [15]. Our main purpose in this study is to extend this scheme to be applied to broad classes of materials and assess its performance. Following Refs. [16,62], the correction energy of the FNV scheme is expressed as

$$E_{\rm FNV} = E_{\rm PC} - q\Delta V_{{\rm PC},q/b}|_{\rm far}. \tag{11}$$

$\Delta V_{{\rm PC},q/b}$ is the potential difference between the defect-induced potential

$$V_{q/b} = V_{{\rm defect},q} - V_{\rm bulk}, \tag{12}$$

and the PC potential $V_{{\rm PC},q}$ [8,15,16,62],

$$\Delta V_{{\rm PC},q/b} = V_{q/b} - V_{{\rm PC},q}. \tag{13}$$

$\Delta V_{{\rm PC},q/b}|_{\rm far}$ is $\Delta V_{{\rm PC},q/b}$ at a place far from the defect in the supercell. Instead of a Gaussian charge originally adopted in Ref. [15] as a model charge for the localized defect in the supercell, we use a PC. This is because the PC model can be readily rewritten in the anisotropic form, and the correction energy can be divided into a physically meaningful long-range Coulomb interaction part and a short-range part [62]. The latter can also be attained with a Gaussian function by redefining the long-range Coulomb interaction energy and alignmentlike term in cubic systems [16].

The second term in Eq. (11) is referred to as potential alignmentlike term [8,15]. An important point is that this alignmentlike term is different from the conventional potential alignment and approximately corresponds to the MP third-order term when the PC model is used [8,62]. When ρ_d has a spherical distribution, which is an assumption of the FNV correction scheme, the defect-induced potential outside of the defect coincides with the PC potential under the open boundary condition, whereas they are different under the periodic boundary condition. This discrepancy is due to the convention of the zero-average potential. Komsa *et al.* have discussed this point in detail in Ref. [8] and derived the relationship $\Delta V_{{\rm PC},q/b}|_{\rm far} = \frac{2\pi Q}{3\varepsilon\Omega}$ in an isotropic medium. This spurious potential shift caused by the periodic boundary condition has to be removed for charged defects, and its correction corresponds to the alignmentlike term. The principal advantage of the FNV scheme is that we do not have to know the details of microscopic screening and its coupling to the actual unscreened or partially screened charge distribution beyond the PC model because these effects are incorporated into the alignmentlike term. Another benefit is that it is applicable to any shapes of supercells, under the assumption that the defect charge is fully contained in the supercell.

Although it was originally proposed to use either neutral defect or pristine bulk as a reference potential for estimating $\Delta V_{{\rm PC},q/b}$, we use the pristine bulk only. This is because the pristine bulk is a reference state of a defective system as with vacuum of a molecular system, and the defect charge and defect-induced potential are defined as charge and potential variations from those of the pristine bulk, respectively. Komsa *et al.* proposed a way to estimate $\Delta V_{{\rm PC},q/b}$ by using the potential of a neutral defect system as a reference, and to perform the conventional potential alignment between the neutral defect and pristine bulk systems [8]. Their approach is conceptually different, but the final correction energy is the same as ours.

D. Application of atomic site potential as a potential marker

Originally, the FNV scheme used planar-averaged electrostatic potential to determine $\Delta V_{{\rm PC},q/b}|_{\rm far}$ [15]. This, however, does not work when atoms far from the defect are strongly shifted from their unrelaxed crystalline positions after geometry optimization. It is especially significant for an ionic host, in which long-range Coulomb interaction is screened by dipoles of polarizable ions. This is demonstrated in Figs. 1(a) and 1(b) that show the planar-averaged defect-induced potential $V_{q/b}$, PC potential $V_{{\rm PC},q}$, and their difference $\Delta V_{{\rm PC},q/b}$ for the unrelaxed and relaxed B vacancy in the -3 charge state ($V_{\rm B}^{-3}$) in c-BN. In the unrelaxed geometry, both $V_{q/b}$ and $V_{{\rm PC},q}$ show a parabolic shape far from the defect, which comes from the homogeneous background charge through the Poisson's equation. Their difference then reaches a plateau between the defect and its periodic image, and $\Delta V_{{\rm PC},q/b}|_{\rm far}$ can be obtained with small uncertainty. On the other hand, $V_{q/b}$ strongly fluctuates in the relaxed geometry reflecting the atomic displacements, whereas $V_{{\rm PC},q}$ remains parabolic. As a result, $\Delta V_{q/b}^{\rm PC}|_{\rm far}$ can not be determined accurately.

An alternative way is to employ atomic site electrostatic potential. This is often utilized for the potential alignment in defect calculations [7,33] as well as determination of ionization potential and band offsets in semiconductors and insulators [30,63,64]. In analogy with Eq. (8), using the principal axis transformation and following derivation of the Ewald scheme, we derive the screened potential at an arbitrary position $\boldsymbol{r} \neq \boldsymbol{0}$ in an anisotropic dielectric as

$$\begin{aligned} &V_{{\rm PC},q}^{\rm aniso}(\boldsymbol{r} \neq \boldsymbol{0}) \\ &= \sum_{\boldsymbol{R}_i} \frac{q}{\sqrt{|\bar{\varepsilon}|}} \frac{{\rm erfc}(\gamma\sqrt{(\boldsymbol{R}_i - \boldsymbol{r})\cdot\bar{\varepsilon}^{-1}\cdot(\boldsymbol{R}_i - \boldsymbol{r})})}{\sqrt{(\boldsymbol{R}_i - \boldsymbol{r})\cdot\bar{\varepsilon}^{-1}\cdot(\boldsymbol{R}_i - \boldsymbol{r})}} - \frac{\pi q}{\Omega\gamma^2} \\ &\quad + \sum_{\boldsymbol{G}_i}^{i\neq 0} \frac{4\pi q}{\Omega} \frac{\exp(-\boldsymbol{G}_i\cdot\bar{\varepsilon}\cdot\boldsymbol{G}_i/4\gamma^2)}{\boldsymbol{G}_i\cdot\bar{\varepsilon}\cdot\boldsymbol{G}_i} \cdot \exp(i\boldsymbol{G}_i\cdot\boldsymbol{r}). \end{aligned} \tag{14}$$

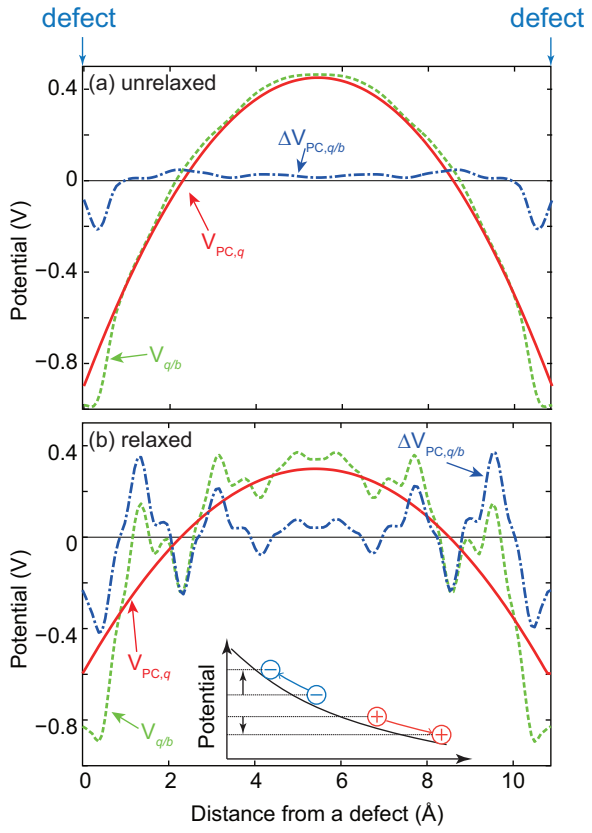

FIG. 1. (Color online) Planar-averaged defect-induced potential $V_{q/b}$, PC potential $V_{\mathrm{PC},q}$, and their difference $\Delta V_{\mathrm{PC},q/b}$ of (a) unrelaxed and (b) relaxed V_{B}^{-3} in c-BN with a $3 \times 3 \times 3$ supercell containing 215 atoms. Inset in (b): Schematic illustration showing the displacements of polarizable ions under the electric field caused by the charged defect.

Compared to the Madelung potential shown in Eq. (8), $\boldsymbol{R}_0$ is included into summation in the first term, and the fourth term in Eq. (8) is removed. This is used for evaluating $\Delta V_{\mathrm{PC},q/b}$ in Eq. (13). We should keep in mind that the farthest atomic site from the defect is not necessarily the best reference for evaluating $\Delta V_{\mathrm{PC},q/b}|_{\mathrm{far}}$. This is because (i) the farthest atom lies between the defect and its periodic images, and non-negligible overlap of defect wave functions might exist in small supercells, and (ii) the displacements of polarizable ions as a result of screening may bias the electrostatic potential as illustrated in the inset of Fig. 1(b). The FNV scheme assumes that an approximately spherical defect charge is fully contained in the supercell. Thus, we instead propose for $\Delta V_{\mathrm{PC},q/b}|_{\mathrm{far}}$ to average $\Delta V_{\mathrm{PC},q/b}$ at the atomic positions in the region outside of the sphere that is in contact with the Wigner-Seiz cell with radius R_{WS} as illustrated in Fig. 2(a). We call this region the sampling region. It is also advantageous that the sampling region does not depend on the choice of the supercell if the Bravais lattice is unchanged. As an example, the atomic site $V_{q/b}$, $V_{\mathrm{PC},q}$, and $\Delta V_{\mathrm{PC},q/b}$ of V_{B}^{-3} in c-BN are shown in Fig. 2(b). $\Delta V_{\mathrm{PC},q/b}$ shows scattering behavior near the defect, but it converges at the outside of R_{WS}.

A disadvantage of the use of the atomic site potential is that the number of atomic sites for determining $\Delta V_{\mathrm{PC},q/b}|_{\mathrm{far}}$ might not be sufficient in small supercells, and non-negligible

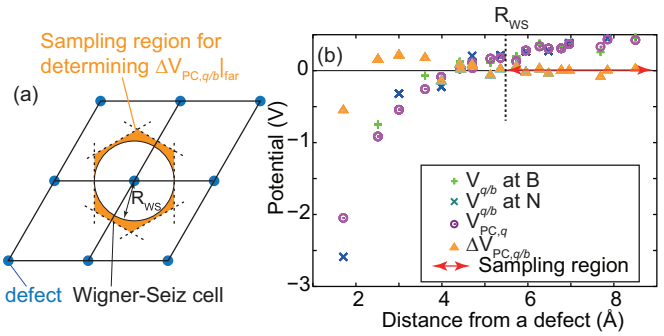

FIG. 2. (Color online) (a) Schematic of the sampling region used for estimating $\Delta V_{\mathrm{PC},q/b}|_{\mathrm{far}}$ by averaging atomic site $\Delta V_{\mathrm{PC},q/b}$ at the region outside of the sphere in contact with the Wigner-Seiz cell. Note that the sampling region depends only on the Bravais lattice of the supercell. (b) $V_{q/b}$, $V_{\mathrm{PC},q}$, and $\Delta V_{\mathrm{PC},q/b}$ at the atomic positions in the supercell of relaxed V_{B}^{-3} in c-BN. The region for averaging $\Delta V_{\mathrm{PC},q/b}$ and its averaged value are expressed in the width and height of the arrow, respectively.

sampling errors might be involved. To check the accuracy, we compare the averaged atomic site $\Delta V_{\mathrm{PC},q/b}|_{\mathrm{far}}$ with planar-averaged $\Delta V_{\mathrm{PC},q/b}|_{\mathrm{far}}$. In Figs. 3(a)–3(d), we show atomic site and planar-averaged $V_{q/b}$, $V_{\mathrm{PC},q}$, and $\Delta V_{\mathrm{PC},q/b}$ of the Mg vacancy (V_{Mg}^{-2}) in MgO and the Si self-interstitial at the tetrahedral site (Si_i^{+2}) in Si. For comparison, we used relatively small $2 \times 2 \times 2$ supercells constructed from the conventional unit cells and did not relax atomic positions. Between the defect and its images, the planar-averaged $\Delta V_{\mathrm{PC},q/b}$ almost converges in both defect systems, indicating the defect charge is well localized in the supercells. $\Delta V_{\mathrm{PC},q/b}|_{\mathrm{far}}$ determined from the atomic site potential at the sampling region are almost the same for V_{Mg}^{-2} in MgO and Si_i^{+2} in Si; the differences are less than 40 meV in both systems. When the cell size increases, these differences and consequently sampling errors drastically reduce, partly owing to the increase of the sampling points for evaluating $\Delta V_{\mathrm{PC},q/b}$.

E. Assessment of the accuracy of the extended FNV scheme for anisotropic materials

Here, we discuss the performance of the extended FNV scheme using the anisotropic PC model. The test calculations were performed for the Ti vacancy (V_{Ti}^{-4}) in β-Li_2TiO_3 [20] and the B antisite defect on N ($\mathrm{B_N^{+2}}$) in h-BN. Their crystal structures are shown in Figs. 4(a) and 4(b). As can be inferred from the layered structures, the dielectric tensors have very different diagonal components as listed in Table I.

Figures 4(c) and 4(d) show the atomic site $V_{q/b}$, $V_{\mathrm{PC},q}$, and $\Delta V_{\mathrm{PC},q/b}$ of V_{Ti}^{-4} in a β-Li_2TiO_3 $2 \times 2 \times 2$ supercell and $\mathrm{B_N^{+2}}$ in an h-BN $8 \times 8 \times 3$ supercell. $V_{q/b}$ widely scatter even at the same distance from the defect, reflecting the anisotropic screening feature. Interestingly, $V_{q/b}$ in $\mathrm{B_N^{+2}}$ can be divided into layer-by-layer components. $\Delta V_{\mathrm{PC},q/b}$ in $\mathrm{B_N^{+2}}$ is almost constant except the immediate vicinity of the defect, indicating that the defect charge is very localized. On the other hand, $\Delta V_{\mathrm{PC},q/b}$ of V_{Ti}^{-4} in β-Li_2TiO_3 is widespread and converges in a region far from the defect.

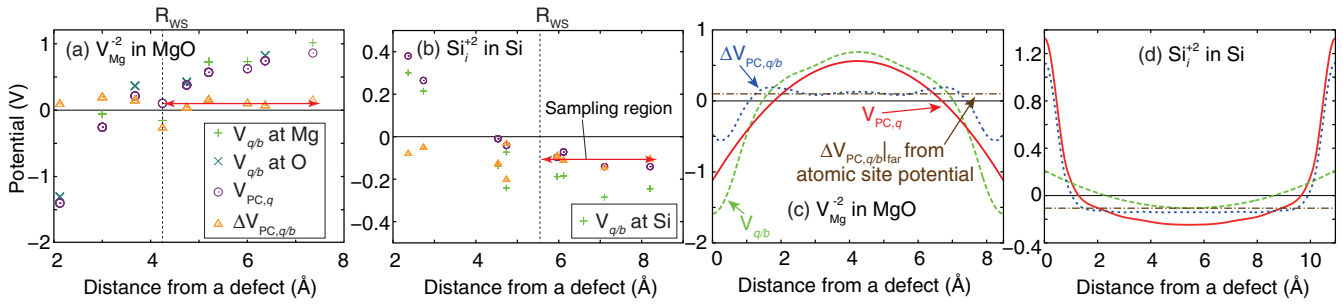

FIG. 3. (Color online) Planar-averaged $V_{q/b}$, $V_{PC,q}$, and $\Delta V_{PC,q/b}$ of unrelaxed (a) V_{Mg}^{-2} and (b) Si_i^{+2} together with $\Delta V_{PC,q/b}|_{far}$ in (c) and (d).

We corrected their formation energies based on Eq. (11). $E_f[V_{Ti}^{-4}]$ in β-Li_2TiO_3 and $E_f[B_N^{+2}]$ in h-BN without corrections, with FNV corrections in the isotropic form, where the average of the diagonal components of the dielectric tensor is used as a dielectric constant $\varepsilon = \langle \varepsilon_{ii} \rangle$, and PC and FNV corrections in the anisotropic form are plotted in Figs. 4(e) and 4(f) for a range of supercell sizes and shapes. As discussed later, the potential alignment is not considered to avoid double counting of the correction term.

Without corrections, $E_f[V_{Ti}^{-4}]$ in β-Li_2TiO_3 widely scatters depending on the supercell size and shape. The isotropic FNV correction with a dielectric constant, which is a typical approximation, does not avail to correct $E_f[V_{Ti}^{-4}]$; in the elongated supercells, it makes $E_f[V_{Ti}^{-4}]$ even worse. On the other hand, the anisotropic PC drastically reduces the cell size/shape dependence of $E_f[V_{Ti}^{-4}]$ as also reported in Ref. [20]. The potential alignmentlike term in the anisotropic FNV scheme corrects the remaining cell size/shape dependence, and it almost vanishes in large supercells. As a result, we see that the extension along the a axis is essential for accurate estimation of $E_f[V_{Ti}^{-4}]$, and the $2 \times 1 \times 1$ 95-atom supercell would be a good compromise for computationally expensive

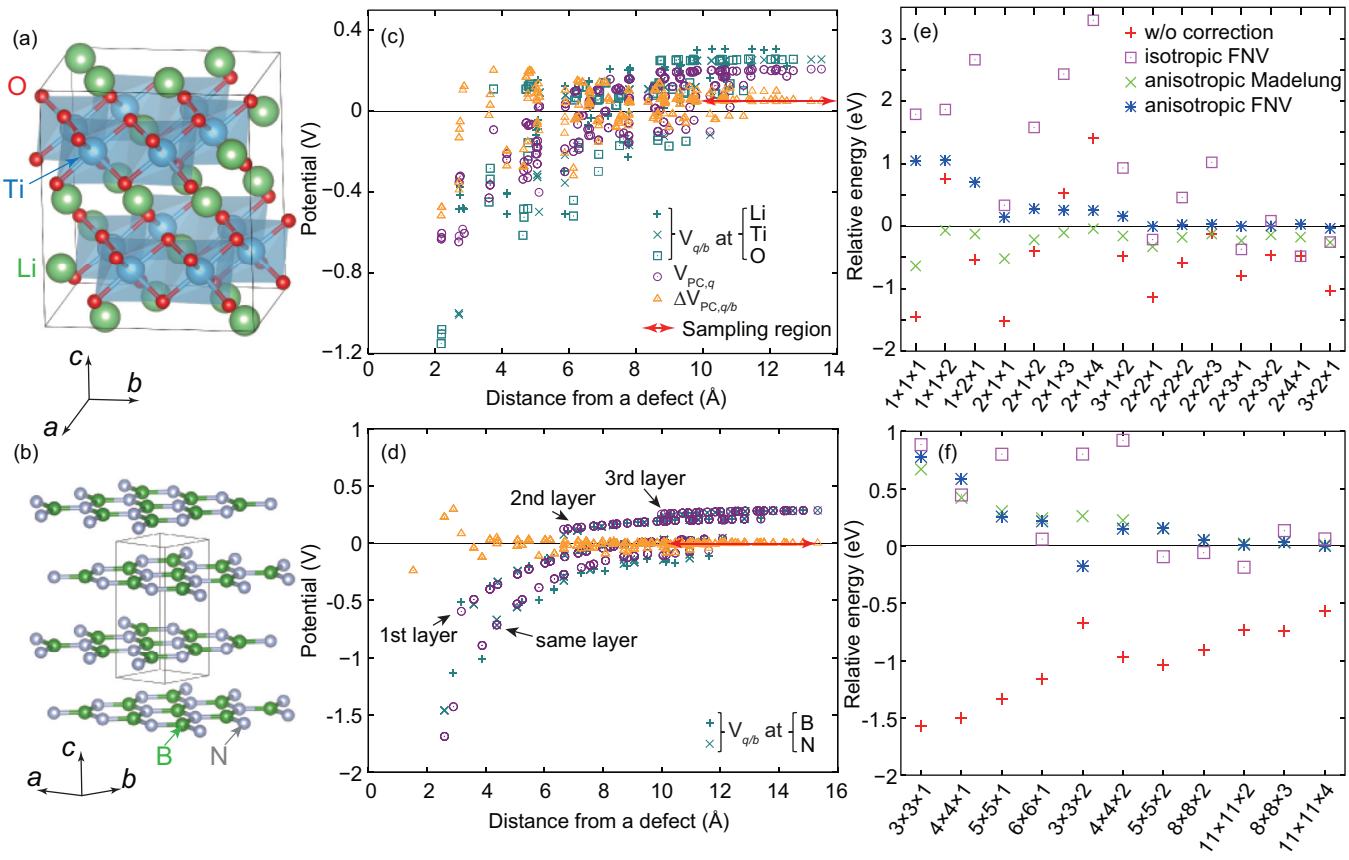

FIG. 4. (Color online) Crystal structures of (a) β-Li_2TiO_3 and (b) h-BN. The unit cells of β-Li_2TiO_3 and h-BN contain 48 and 4 atoms, respectively. $V_{q/b}$, $V_{PC,q}$, and $\Delta V_{q/b}^{PC}$ at the atomic sites for (c) V_{Ti}^{-4} in the $2 \times 2 \times 2$ supercell of β-Li_2TiO_3 (383 atoms) and (d) B_N^{+2} in the $8 \times 8 \times 3$ supercell of h-BN (768 atoms). Relative formation energies of (e) V_{Ti}^{-4} and (f) B_N^{+2} as a function of the supercell size and shape. Zeros are set to the formation energies calculated with the largest supercells and anisotropic FNV corrections. Atomic relaxations are considered in all cases.

first-principles calculations such as hybrid functional calculations. Similarly, the anisotropic PC correction significantly improves $E_f[B_N^{+2}]$ in h-BN, but the alignmentlike term is quite small due to the small second radial moment (see Sec. V). $E_f[B_N^{+2}]$ is systematically overestimated when the c axis is not expanded in the supercell. In this case, BN sheets with and without defects alternate layer by layer, and it would not be appropriate to use a static dielectric constant $\varepsilon^{\rm ele} + \varepsilon^{\rm ion}$ along the c direction. Thus, good compromise for $E_f[B_N^{+2}]$ would be a $4 \times 4 \times 2$ 128-atom supercell, which is expected to have an error less than 0.15 eV.

IV. POTENTIAL ALIGNMENT REVISITED

As mentioned above, there is a longstanding controversy over the need for a potential alignment and how best to formulate it. We here demonstrate that the potential alignment is not needed under the assumption that the image-charge correction is properly constructed. Indeed, some authors refrain from adopting both potential alignment *and* image-charge corrections because the former might contain a part of the latter, leading to double counting of spurious Coulomb interaction corrections [17,24,65]. As indicated in Eq. (4), image-charge corrections remove the spurious Coulomb potential caused by the defect images and background charge, and shifts the potential from $V_{{\rm defect},q}$ to $V_{{\rm isolated},q}$. Then, $V_{{\rm isolated},q} = V_{{\rm defect},q} + V_{\rm cor} = V_{\rm bulk} + V_{q/b} + V_{\rm cor}$, and $V_{q/b} + V_{\rm cor}$ is the potential induced by a single defect. The proper potential alignment is achieved at a point infinitely far from the defect, and $\lim_{|\boldsymbol{r}|\to\infty}(V_{q/b} + V_{\rm cor}) = 0$. Hence, after adopting the image-charge correction, the potential of the supercell with a single defect is aligned to the bulk potential, indicating that the potential alignment is unnecessary for estimating the charged defect formation energy, i.e., $\Delta v = 0$ in Eq. (1).

The situation is analogous to an isolated charged ion in a cell under the periodic boundary condition, where the electrostatic potential reference is not the pristine bulk but vacuum. Even in this case, the total energy depends on the undetermined shift of electrostatic potential, and thus the potential at vacuum must be aligned to be zero. Because the screening charge is absent and the ionic charge $\rho_{\rm ion}$ is well defined, $Q = \int r^2 \rho_{\rm ion}(\boldsymbol{r}) d\boldsymbol{r}$ is calculated exactly. Figure 5(a) shows the planar-averaged electrostatic potential of a Si^+ ion obtained from a self-consistent calculation with the PBE-GGA and of the PC model with the +1 charge, and their difference in a 10 Å × 10 Å × 10 Å cell. Around the Si^+ ion, the electrostatic potential is substantially different from the PC potential because of a finite distribution of the electrons. It, however, becomes almost parallel to the PC potential at a distance of ∼2 Å from the ion, and the difference converges to a constant of $\frac{2\pi Q}{3L^3}$. Therefore, after applying the PC correction and alignmentlike correction, i.e., the FNV correction, the electrostatic potential far from the Si^+ ion changes to zero, meaning that the outermost potential from the Si^+ ion is already aligned to zero. We find that the alignmentlike correction is almost the same as the MP third-order correction via an explicit calculation of Q in this atomic case (the difference is 0.02 meV in the 10 Å × 10 Å × 10 Å cell). Figure 5(b) shows the cell-size dependence of the ionization energy of the Si atom. Note also that the ionization energy with the FNV correction (sum of the PC correction and potential alignmentlike correction) does not show the cell-size dependence.

We emphasize that when the potential alignment is performed at a particular atomic site *before* the image-charge correction, which is the most commonly used potential alignment, a part of the PC correction is included in addition to the alignmentlike term. This can be understood by writing the potential alignment term with Eq. (13) as

$$\begin{aligned} -qV_{q/b}(\boldsymbol{r}) &= -q\left[V^{\rm iso}_{{\rm PC},q}(\boldsymbol{r}) + \Delta V_{{\rm PC},q/b}\big|_{\rm far}\right] \\ &= \alpha(\boldsymbol{r}) E^{\rm iso}_{\rm PC} - q\Delta V_{{\rm PC},q/b}|_{\rm far}, \end{aligned} \tag{15}$$

where the potential alignment is performed at $\boldsymbol{r}$ outside of the defect; thus, $\Delta V_{{\rm PC},q/b}$ reaches a plateau of $\Delta V_{{\rm PC},q/b}|_{\rm far}$. Fractions α of the PC correction included in the potential alignment are calculated from $\alpha(\boldsymbol{r}) = -qV^{\rm iso}_{{\rm PC},q}(\boldsymbol{r})/E^{\rm iso}_{\rm PC}$ in an isotropic medium. Note that α depends only on the fractional coordinates and supercell shape. Figure 5(c) shows α at (0.5, 0, 0), (0.5, 0.5, 0), and (0.5, 0.5, 0.5) in fractional coordinates in cubic systems. For instance, when the potential at (0.5, 0.5, 0.5) is aligned to the bulk potential, 57% of the PC correction and 100% of the alignmentlike term are incorporated via Eq. (15). This is demonstrated for the Si ionization energy. Figure 5(b) shows the corrected ionization energies by the potential alignment at (0.5, 0.5, 0.5). They have cell-size dependence linear to L^{-1}, and the rest of the correction energy corresponds to 43% of the PC correction. 41% and 7% of the PC correction are included if the potential alignment is made at (0.5, 0.5, 0) and (0.5, 0, 0), respectively.

Lany and Zunger have reported that after the potential alignment, the third-order contribution of the image-charge correction vanishes and only 65% of the first-order contribution remains for various defects with different charge states in GaAs [7,10]. They explained the unexpected proportionality by calculating the second radial moment in the MP third-order term using the total charge density difference between the charged and neutral DFT calculations, which includes the defect charge, screening charge, and counterscreening charge. However, their explanation contradicts with the fundamental assumption of the MP correction that the defect charge ρ_d does not include screening and counterscreening charges as pointed out by Komsa *et al.* [8] and Lambrecht [4].

Here, we provide another explanation for the L^{-1} behavior after potential alignment. We can rewrite the FNV correction energy with Eq. (15) as

$$\begin{aligned} E_{\rm FNV} &= E_{\rm PC} - q\Delta V_{{\rm PC},q/b}|_{\rm far} \\ &= [1 - \alpha(\boldsymbol{r})]E_{\rm PC} - qV_{q/b}(\boldsymbol{r}). \end{aligned} \tag{16}$$

Supposing that the FNV scheme successfully corrects the defect formation energy, namely, no cell-size dependence remains after the FNV correction, $[1 - \alpha(\boldsymbol{r})]E_{\rm PC}$ should remain after the potential alignment. Then, after the potential alignment is performed at the same fractional coordinates in the supercells with the same shape, the defect formation energies show L^{-1} dependence. Although in Ref. [10] the potential alignment was achieved by averaging the potential offset at atomic sites except for the immediate neighbors of the defect and thus α is unclear, the absence of the third-order contribution would be explained with Eq. (16). Our results support this as shown in the next section.

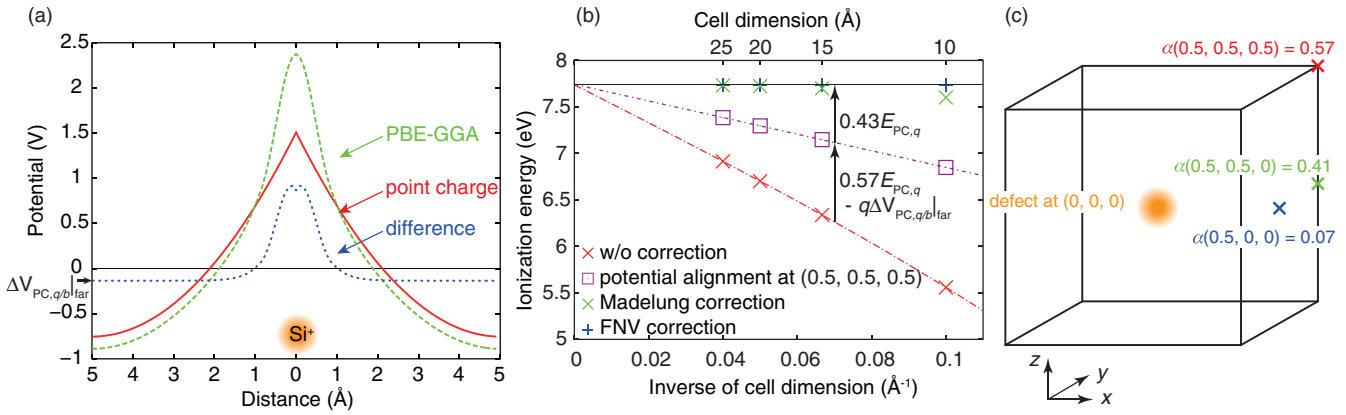

FIG. 5. (Color online) (a) Planar-averaged electrostatic potential of a Si^{+} ion calculated with the PBE-GGA located in a 10 Å × 10 Å × 10 Å cell, the PC potential with the +1 charge, and their difference. (b) Cell-size dependence of the uncorrected and corrected ionization energy of a Si atom, $E(\mathrm{Si}^{+}\ \mathrm{ion}) - E(\mathrm{Si\ atom}) + E_{\mathrm{cor}}$. The ionization energy becomes almost independent of the cell dimension after applying both the PC correction and alignmentlike correction (the FNV correction scheme). (c) The fractions α of the PC correction implicitly included in the potential alignment at three points written in fractional coordinates in the cubic cell in an isotropic medium. Note that the alignmentlike term is fully included in the potential alignment at any point (see text).

V. APPLICATIONS TO DEFECTS IN DIVERSE MATERIALS

A. Systematic evaluation of the extended FNV scheme

To assess the accuracy of the extended FNV scheme, we calculated the formation energies of defects in a variety of host materials: V_{Zn}^{-2}, V_{O}^{+2}, and the Zn interstitial at the octahedral site (Zn_i^{+2}) in ZnO [7,24,61,66–68], V_{Mg}^{-2} and V_{O}^{+2} in MgO [68,69], V_{Al}^{-3} and V_{O}^{+2} in Al_2O_3 [68,70], V_{Hf}^{-4} and V_{O}^{+2} on the threefold-coordinated O site in HfO_2, V_{B}^{-3} and a defect complex of Ce on the N site coupling with neighboring four B vacancies ($\mathrm{Ce_N}$-$4V_{\mathrm{B}}^{-6}$) in c-BN [40], Si_i^{+2} and V_{Si}^{+2} in Si [17,57,71–73], V_{As}^{+3} in GaAs [7,10,74], and V_{C}^{+2} in diamond [75]. This covers a wide range of crystal structures, local structures, chemistry (covalency and ionicity), and defect types (vacancies, interstitials, and substitutional impurities). We checked that these defects do not have delocalized perturbed host states with and without electron occupation for donorlike and acceptorlike states, respectively, which is a prerequisite of the electrostatics-based corrections including the FNV scheme; perturbed host states require special treatments, e.g., by considering effective defect charges [8,24]. The uncorrected and corrected defect formation energies with the PC model, FNV scheme with an isotropic approximation, and extended FNV scheme are shown in Fig. 6. The uncorrected defect formation energies are extrapolated to the dilute limit by fitting a function of the form $aN_{\mathrm{atoms}}^{-1} + bN_{\mathrm{atoms}}^{-1/3} + c$, where N_{atoms} is the number of atoms in the supercell before introducing a defect, when the cell dimension is isotropically expanded. We find that the cell-size dependencies of the FNV corrected defect formation energies with large supercells are rather small, indicating the validity as the reference energies.

The PC corrections basically improve the defect formation energies. Especially, V_{Zn}^{-2} and Zn_i^{+2} in ZnO and V_{B}^{-3} in c-BN are well corrected. However, it overshoots the energy of V_{O}^{+2} in ZnO, MgO, Al_2O_3, and HfO_2, V_{Si}^{+2} in Si, V_{As}^{+3} in GaAs, and V_{C}^{+2} in diamond. The FNV corrections, which are the sum of the PC correction and the alignmentlike term, greatly improve the defect formation energies in most cases, but $E[V_{\mathrm{Zn}}^{-2}]$ and $E[\mathrm{Zn}_i^{+2}]$ in ZnO are overshot. $E[V_{\mathrm{C}}^{+2}]$ in diamond calculated with the HSE06 hybrid functional are also well corrected by the FNV scheme.

To compare the FNV corrected energies with an averaged dielectric constant and a dielectric tensor is helpful to see how large an error is when using the isotropic FNV scheme for anisotropic systems. Contrary to the defects in β-Li_2TiO_3 and h-BN, the defects in ZnO, Al_2O_3, and HfO_2 do not show a large difference between the isotropic and anisotropic FNV schemes. Therefore, using an averaged dielectric constant would be a good approximation for these materials.

As discussed in Sec. III, essential assumptions are (i) the defect charge is fully contained in the supercell, and (ii) its distribution does not have cell-size dependence. The absence of the delocalized perturbed host states is just an essential condition and not sufficient to confirm the assumptions. The obvious cell-size dependence of $E[V_{\mathrm{Si}}^{+2}]$ in Si with FNV correction may reflect violation of the assumption. To check this, we plotted $\Delta V_{\mathrm{PC},q/b}|_{\mathrm{far}}\Omega$ in Fig. 7. Supposing that the defect charge remains the same in different supercells, $\Delta V_{\mathrm{PC},q/b}|_{\mathrm{far}}\Omega \approx \frac{2\pi Q}{3\varepsilon}$ must be constant because Q is constant.

One can see that $\Delta V_{\mathrm{PC},q/b}|_{\mathrm{far}}\Omega$ are mainly positive in vacancies and negative in interstitials. This can be qualitatively understood as follows. Supposing the unrelaxed geometry, Table II shows the sign of second radial moment Q and

TABLE II. Sign of charge q, second radial moment Q, and alignmentlike term $-q\Delta V_{\mathrm{PC},q/b}|_{\mathrm{far}}$ for charged vacancies and interstitials in a $\mathrm{A}^{+N}\mathrm{B}^{-N}$ binary compound.

	V_{A}^{-N}	V_{B}^{+N}	X_i^{+N}	X_i^{-N}
q	−	+	+	−
Q, $\Delta V_{\mathrm{PC},q/b}\|_{\mathrm{far}}$	+	+	−	−
$-q\Delta V_{\mathrm{PC},q/b}\|_{\mathrm{far}}$	+	−	+	−

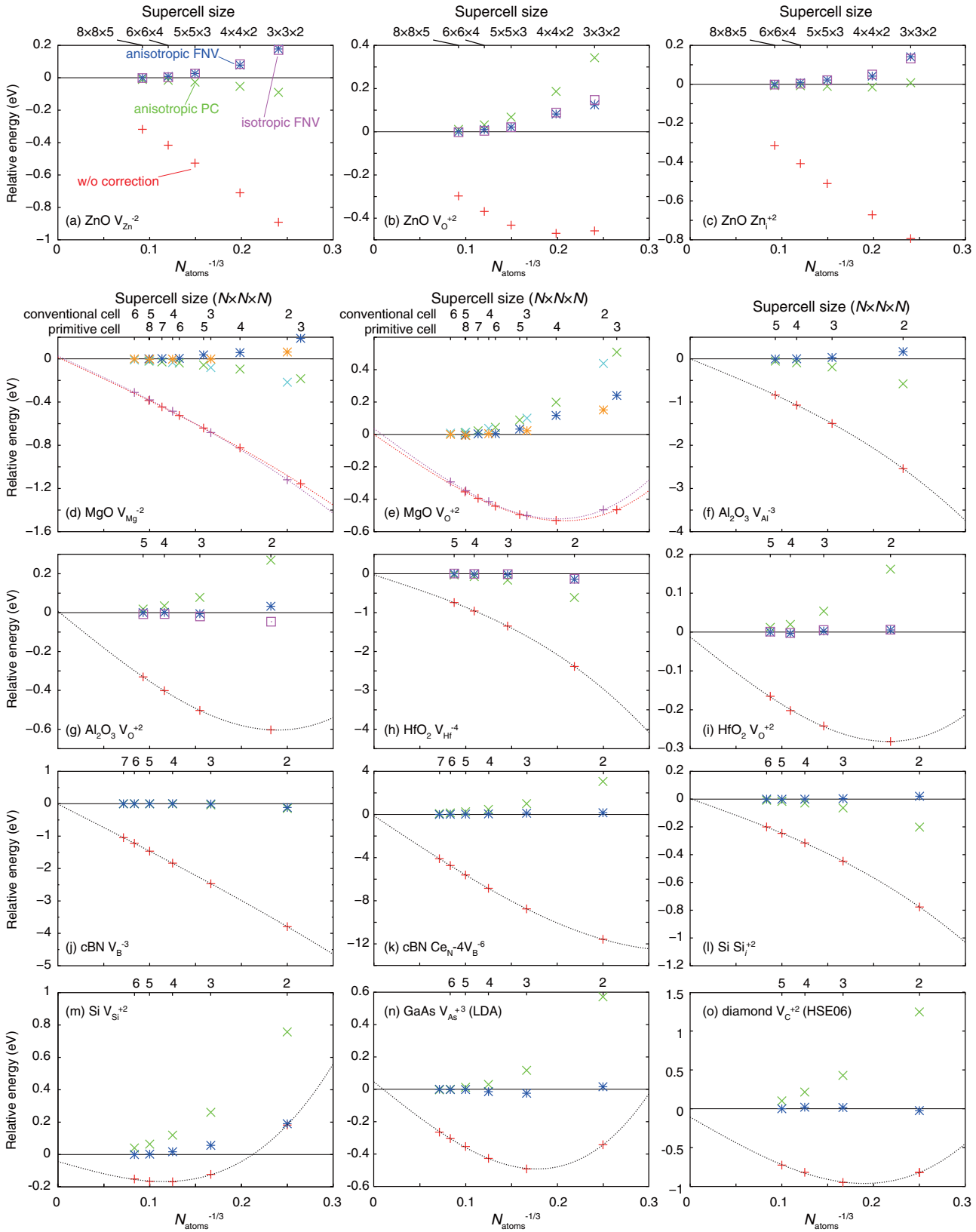

FIG. 6. (Color online) Relative formation energies of (a) V_{Zn}^{-2}, (b) V_O^{+2}, and (c) Zn_i^{+2} in ZnO, (d) V_{Mg}^{-2} and (e) V_O^{+2} in MgO, (f) V_{Al}^{-3} and (g) V_O^{+2} in Al_2O_3, (h) V_{Hf}^{-4} and (i) V_O^{+2} in HfO_2, (j) V_B^{-3} and (k) Ce_N-$4V_B^{-6}$ in c-BN, and (l) Si_i^{+2} and (m) V_{Si}^{+2} in Si, (n) V_{As}^{+3} in GaAs, and (o) V_C^{+2} in diamond with atomic relaxation considered. Zeros are set to the anisotropic FNV corrected defect formation energies calculated with the largest supercells. The horizontal axis is taken as the inverse of the cube root of the number of atoms. In the cases where the cell dimension is isotropically expanded, the uncorrected defect formation energies are fitted with a function of $aN_{\mathrm{atoms}}^{-1} + bN_{\mathrm{atoms}}^{-1/3} + c$.

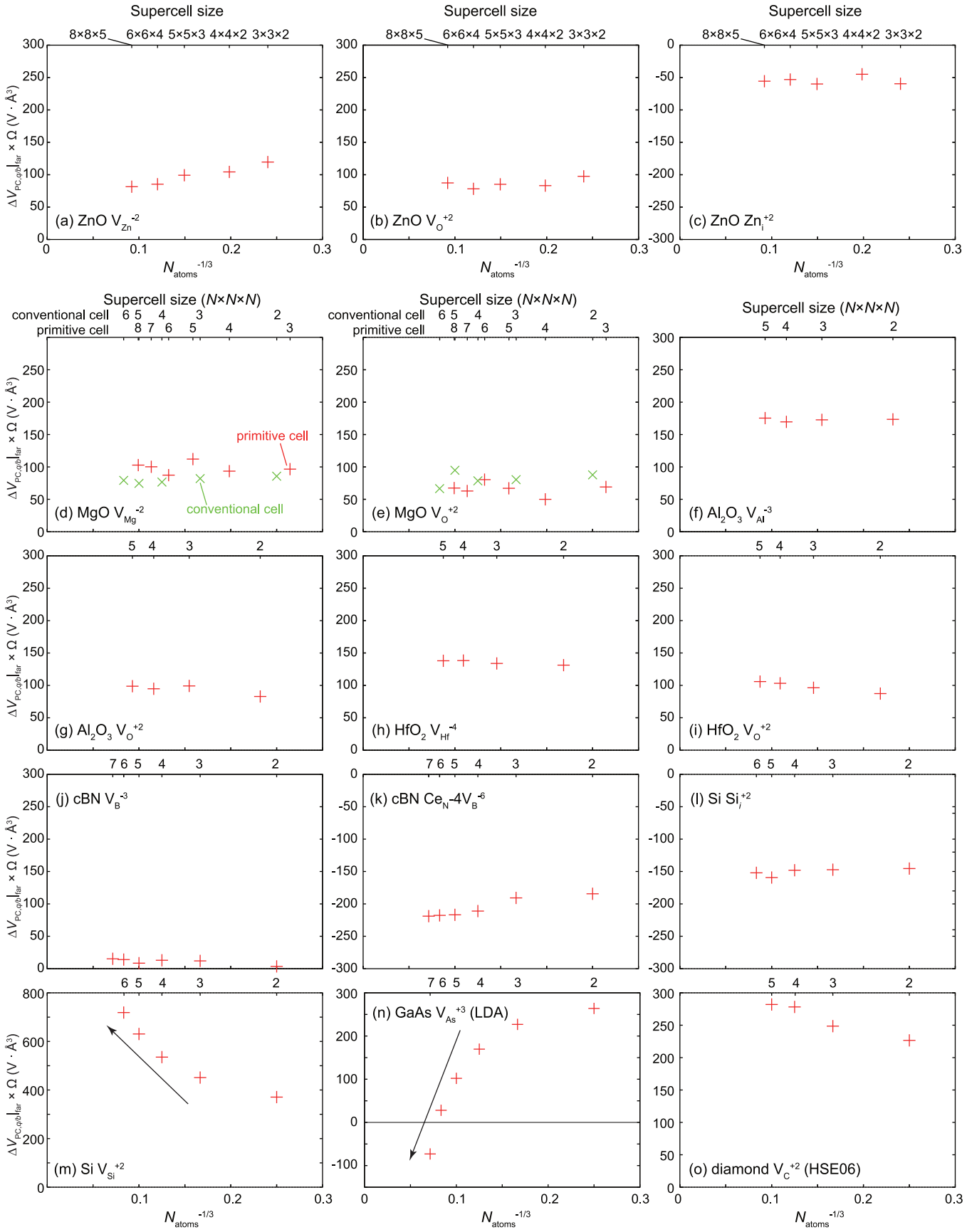

FIG. 7. (Color online) $\Delta V_{PC,q/b}|_{far}\Omega$ of the defects shown in Fig. 6. For comparison, the scales of the vertical axes are set to be the same except for V_{Si}^{+2} in Si and V_{As}^{+3} in GaAs. Large changes of $\Delta V_{PC,q/b}|_{far}\Omega$ are indicated by arrows for guides to the eye.

alignmentlike term $-q\Delta V_{\mathrm{PC},q/b}|_{\mathrm{far}}$ for charged vacancies and interstitials. In the case of vacancies, the valence and core electrons of the removed atom are also removed, and hence $\rho_d(\boldsymbol{r}\neq\boldsymbol{0})>0$ and $Q=\int r^2\rho_d(\boldsymbol{r})d\boldsymbol{r}>0$, because the nucleus of the removed atom located at the defect site $\boldsymbol{r}=\boldsymbol{0}$. On the contrary, in the case of interstitials, due to the electrons of the interstitial atom, $\rho_d(\boldsymbol{r}\neq\boldsymbol{0})<0$ and $Q<0$. The alignmentlike term $-q\Delta V_{\mathrm{PC},q/b}|_{\mathrm{far}}$ of negatively (positively) charged vacancies or positively (negatively) charged interstitials is then positive (negative) as listed in Table. II.

Interestingly, $\Delta V_{\mathrm{PC},q/b}|_{\mathrm{far}}\Omega$ of V_{O}^{+2} are around 100 [$V\cdot$ Å^3] in any binary oxide in this study, and that of V_{B}^{+3} in c-BN is very small, reflecting a significantly small B^{3+} ionic radius. $\Delta V_{\mathrm{PC},q/b}|_{\mathrm{far}}\Omega$ are almost constant except for V_{Si}^{+2} in Si and V_{As}^{+3} in GaAs; their $\Delta V_{\mathrm{PC},q/b}|_{\mathrm{far}}\Omega$ relate to the change of the defect charge distribution as a function of supercell size. In other words, they violate the assumptions of electrostatics-based image-charge correction. In these two cases, however, the defect formation energies are better corrected than PC corrected ones, although the FNV corrected energies still have small cell-size dependence even with large supercells. The energy and atomic structure of V_{Si}^{+2} are notoriously dependent upon supercell size and k-point sampling [71,73]. In fact, Γ-only k point sampling is not sufficient even with a 1726-atom supercell, and Monkhorst-Pack [76] $2\times2\times2$ k-point mesh was adopted in this study. This would be because the defect charge immersed in the valence band spreads widely, and leads to the erroneous defect-defect interactions. Indeed, planar-averaged $\Delta V_{\mathrm{PC},q/b}|_{\mathrm{far}}$ in the unrelaxed geometry does not reach a plateau between the defect and its image even with a 1726-atom supercell. As a result, $\Delta V_{\mathrm{PC},q/b}|_{\mathrm{far}}\Omega$ increases as the supercell gets larger and larger, and more defect charge is contained. The situation of $E[V_{\mathrm{As}}^{+3}]$ in GaAs is the same although the influence on the energy is rather small and the energies are well corrected with the FNV scheme even with small supercells. Note that the same trend is observed even with the Ga PAW potential including $3d$ electrons in the valence.

For V_{Mg}^{-2} and V_{O}^{+2} in MgO, we calculated the defect formation energies with two types of supercells constructed from conventional and primitive cells, respectively, which have simple cubic (sc) and face-centered-cubic (fcc) defect allocations [10]. Intuitively, the fcc supercells seem suited for defect calculations since the defect-defect distance is longer than that of the sc supercells in the same volume because of the larger coordination number in the fcc allocation. Both $E[V_{\mathrm{Mg}}^{-2}]$ and $E[V_{\mathrm{O}}^{+2}]$ are, however, more accurately calculated with the sc supercells. The reason is unclear but the defect-defect interactions might be enhanced in fcc supercells. Such behavior has also been observed in V_{As}^{+3} in GaAs [10].

The absolute error is of importance in practice, and thus we plot the relative defect formation energies calculated with small supercells containing around 100 atoms in Fig. 8. Such small supercells are convenient for advanced first-principles calculations. It is found that the defect formation energies are excellently corrected by the extended FNV scheme and the differences from those in the dilute limit are less than 0.2 eV in our test set. Surprisingly, the errors do not largely depend on the defect charge as Freysoldt *et al.* pointed out in Ref. [15].

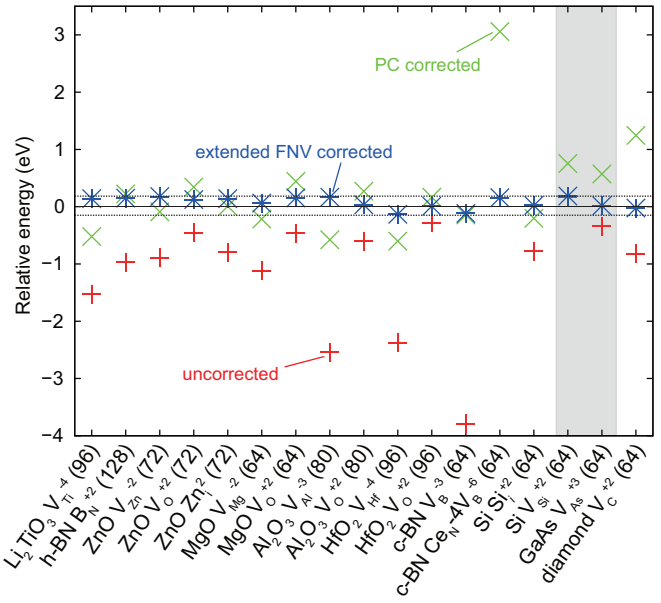

FIG. 8. (Color online) Relative defect formation energies estimated with supercells containing less than 100 atoms except for B_{N}^{+2} antisite defects in h-BN, compared to extended FNV corrected energies estimated with the largest supercells. Atomic relaxation is considered in all cases. The uncorrected energy of Ce_{N}-$4V_{\mathrm{B}}^{-6}$ in c-BN is -11.6 eV. The defects in the shaded area have large cell-size dependencies of $\Delta V_{\mathrm{PC},q/b}|_{\mathrm{far}}\Omega$, indicating violation of the assumption that the defect charge distribution in the supercell is the same as the isolated one. Note that the corrected energies with the extended FNV scheme are located within ±0.2 eV.

The potential alignment discussed in Sec. IV is also reviewed with Ce_{N}-$4V_{\mathrm{B}}^{-6}$ in c-BN, Si_i^{+2} in Si, and V_{As}^{+3} in GaAs in Fig. 9. The energies corrected with the potential alignment at the farthest atomic site from the defect and its images have nearly linear dependence against L^{-1}. The deviations from the linear dependence are, however, larger than that of the Si^+ ionization energy shown in Fig. 5(b). This is because the farthest atoms do not always locate at (0.5, 0.5, 0.5) of the supercells. For instance, such atoms locate at (0.5, 0.5, 0.5) when N in the N^3-fold Si_i supercell is an odd number, but it does not when N is an even number. One can find that the sum of the conventional potential alignment and $1-\alpha$ of the PC correction energy almost recovers the FNV corrected energies, similar to the Si ionization energy in Sec IV. Indeed, they must be the same based on Eq. (16), and the remaining differences correspond to the difference in potential sampling methods; the conventional potential alignment is performed at the farthest atomic site, whereas the FNV correction is performed with the potential in the sampling region in this study.

B. Sources of remaining errors

The FNV scheme can correct the defect formation energies up to the L^{-3} order. We here discuss the origins of the remaining error. The error sources considered are as follows: (i) The defect charge spills out from the supercell. (ii) The defect charge distribution is affected by the spurious potential caused by the image charges and background charge [12]. (iii) Sampling error for the potential alignmentlike term. (iv)

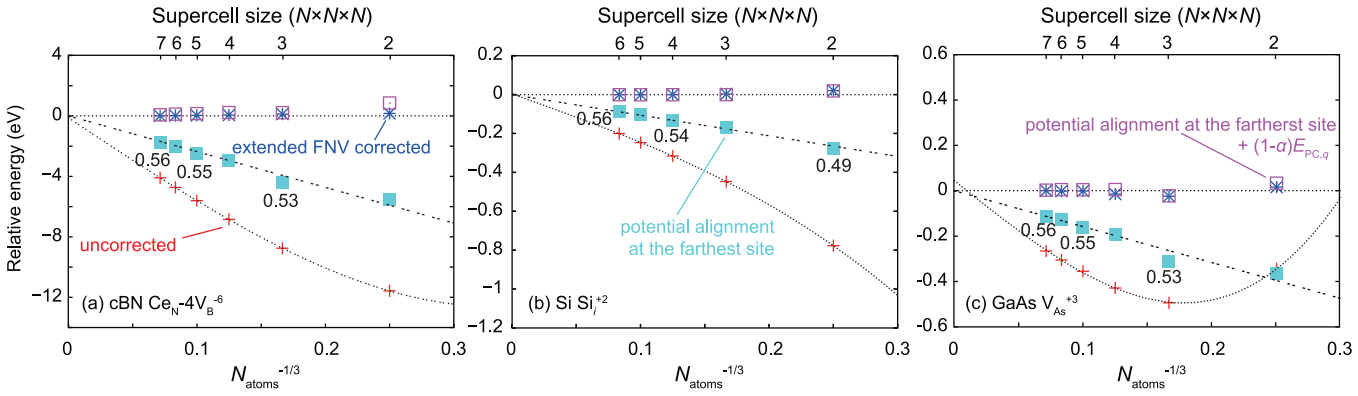

FIG. 9. (Color online) Relative formation energies of (a) Ce_N-$4V_B^{-6}$ in c-BN, (b) Si_i^{+2} in Si, (c) V_{As}^{+3} in GaAs, and their energies corrected with the extended FNV scheme, conventional potential alignment, and potential alignment plus $[1-\alpha(\boldsymbol{r})]E_{PC}$. The potential alignment was performed at the farthest atomic site. In the cases where the farthest atoms locate at (0.5, 0.5, 0.5), $\alpha = 0.57$. Otherwise, α values are shown.

Energy correction with L^{-5} or higher orders. (v) Defect-induced dipoles, which contribute to decrease the formation energy as shown in Eq. (10). (vi) Defect-induced elastics, which contributes to increase the formation energy.

(i)–(iii) can be checked with $\Delta V_{PC,q/b}|_{far}\Omega$ as shown in Fig. 7. (iv) would be dominant when fitting with a function of the form $aN_{atoms}^{-1} + bN_{atoms}^{-1/3} + c$ works poorly. (v) may be only related to the defects in ZnO without an inversion symmetry in this study. The omission of the leading dipole term, however, should underestimate the defect formation energies and this is not true for the defects in ZnO. Roughly estimating, we calculate the dipole energy of the charges $\pm e$ separated 0.5 Å from each other ($\boldsymbol{p} = 0.5 \cdot \boldsymbol{z}$ [$e\cdot$ Å]) in the $4\times4\times2$ supercell of ZnO ($\Omega = 1590$ Å^3) with a theoretical dielectric constant $\varepsilon = \langle\varepsilon_{ii}\rangle = 10.64$, and obtain $\frac{2\pi \boldsymbol{p}^2}{3\varepsilon\Omega} = 5.6$ meV, which is negligibly small compared to the remaining error of the defects in ZnO. Only (vi) is not explicitly dependent on q. Since the remaining errors after the extended FNV correction are not strongly dependent on the defect charges, (vi) might be a main error source for the defects localized in the supercell. Note that the lattice optimization of the defective supercell is not useful to reduce the elastic energy in general because the spurious elastic interactions occur under the periodic boundary condition, and can underestimate the defect formation energy especially in the low-symmetry supercell. A combination of first-principles calculations and elastic theory might resolve this issue [77].

VI. CONCLUSIONS

In this paper, we have discussed electrostatics-based finite-cell-size corrections for first-principles point defect calculations under the periodic boundary condition. In the beginning, the PC correction that is the leading term of the image-charge correction has been reviewed in detail. Then, we have revisited the higher-order correction term $O(L^{-3})$ appearing in the MP and FNV schemes, and proposed a way to extend the FNV scheme to be applicable to a wider variety of materials, especially with low dimensionality. First, we have adopted the atomic site potential for determining the potential offset between the defect-induced potential and PC potential, and compared it with the planar-averaged potential. Second, we have described a PC model with a dielectric tensor for evaluating long-range Coulomb interactions. The anisotropic FNV scheme has been tested with V_{Ti}^{-4} in β-Li_2TiO_3 and B_N^{+2} in h-BN, and their formation energies are found to be well corrected.

The potential alignment, which has been discussed by many authors, has also been revisited in Sec. IV. We have concluded that the potential alignment is unnecessary when the image-charge correction is properly constructed. This is confirmed by calculating the ionization energy of the Si atom in the atomic case. In addition, the correspondence of the FNV scheme to the MP scheme is also confirmed in this limit. We also have discussed the physical meaning of the conventional potential alignment, and found that it contains a part of the PC correction energy and 100% of the alignmentlike term of the FNV scheme. This would be the origin of the absence of the L^{-3} order term and reduction of the L^{-1} order term after applying the potential alignment previously reported [10].

In Sec. V, we have tested the accuracy of the extended FNV scheme with a test set composed of 17 defects in 10 materials, and found that it systematically improves the defect formation energies. The signs of the second radial moment Q and alignmentlike term $-q\Delta V_{PC,q/b}|_{far}$ have also been discussed. The corrected defect formation energies with -6 to $+3$ charges calculated with around 100-atom supercells are within ±0.2 eV compared to those in the dilute limit. We believe that the extended FNV scheme is a powerful tool in practice for correcting defect formation energies under the assumption that the defect charges are fully contained in the supercells.

ACKNOWLEDGMENTS

We thank A. Seko and M. Choi for valuable discussions, and the referees for reading our manuscript carefully. This work was supported by the MEXT Elements Strategy Initiative to Form Core Research Center "Tokodai Institute for Element Strategy (TIES)" and a Grant-in-Aid for Scientific Research on Innovative Areas "Nano Informatics" (Grant No. 25106005) from JSPS. Computing resources of ACCMS at Kyoto University were used in this work. The visualization of crystal structures was performed with VESTA [78].

[1] C. Freysoldt, B. Grabowski, T. Hickel, J. Neugebauer, G. Kresse, A. Janotti, and C. G. Van de Walle, Rev. Mod. Phys. **86**, 253 (2014).
[2] C. G. Van de Walle and J. Neugebauer, J. Appl. Phys. **95**, 3851 (2004).
[3] R. M. Nieminen, Modell. Simul. Mater. Sci. Eng. **17**, 084001 (2009).
[4] W. R. L. Lambrecht, Phys. Status Solidi B **248**, 1547 (2010).
[5] J. Heyd, G. E. Scuseria, and M. Ernzerhof, J. Chem. Phys. **118**, 8207 (2003).
[6] A. V. Krukau, O. A. Vydrov, A. F. Izmaylov, and G. E. Scuseria, J. Chem. Phys. **125**, 224106 (2006).
[7] S. Lany and A. Zunger, Phys. Rev. B **78**, 235104 (2008).
[8] H.-P. Komsa, T. T. Rantala, and A. Pasquarello, Phys. Rev. B **86**, 045112 (2012).
[9] L. Kleinman, Phys. Rev. B **24**, 7412 (1981).
[10] S. Lany and A. Zunger, Modell. Simul. Mater. Sci. Eng. **17**, 084002 (2009).
[11] M. Leslie and N. J. Gillan, J. Phys. C: Solid State Phys. **18**, 973 (1985).
[12] G. Makov and M. C. Payne, Phys. Rev. B **51**, 4014 (1995).
[13] P. A. Schultz, Phys. Rev. Lett. **84**, 1942 (2000).
[14] C. W. M. Castleton, A. Höglund, and S. Mirbt, Phys. Rev. B **73**, 035215 (2006).
[15] C. Freysoldt, J. Neugebauer, and C. G. Van de Walle, Phys. Rev. Lett. **102**, 016402 (2009).
[16] C. Freysoldt, J. Neugebauer, and C. G. Van de Walle, Phys. Status Solidi B **248** (2011).
[17] S. E. Taylor and F. Bruneval, Phys. Rev. B **84**, 075155 (2011).
[18] N. D. M. Hine, K. Frensch, W. M. C. Foulkes, and M. W. Finnis, Phys. Rev. B **79**, 024112 (2009).
[19] R. Rurali and X. Cartoixà, Nano Lett. **9**, 975 (2009).
[20] S. T. Murphy and N. D. M. Hine, Phys. Rev. B **87**, 094111 (2013).
[21] W. M. C. Foulkes, L. Mitas, R. J. Needs, and G. Rajagopal, Rev. Mod. Phys. **73**, 33 (2001).
[22] S. B. Zhang, S.-H. Wei, and A. Zunger, Phys. Rev. B **63**, 075205 (2001).
[23] E. R. Batista, J. Heyd, R. G. Hennig, B. P. Uberuaga, R. L. Martin, G. E. Scuseria, C. J. Umrigar, and J. W. Wilkins, Phys. Rev. B **74**, 121102 (2006).
[24] F. Oba, A. Togo, I. Tanaka, J. Paier, and G. Kresse, Phys. Rev. B **77**, 245202 (2008).
[25] A. Alkauskas, P. Broqvist, and A. Pasquarello, Phys. Rev. Lett. **101**, 046405 (2008).
[26] F. Bruneval, Phys. Rev. Lett. **103**, 176403 (2009).
[27] P. Rinke, A. Janotti, M. Scheffler, and C. G. Van de Walle, Phys. Rev. Lett. **102**, 026402 (2009).
[28] S. Lany and A. Zunger, Phys. Rev. B **81**, 113201 (2010).
[29] W. Chen and A. Pasquarello, Phys. Rev. B **86**, 035134 (2012).
[30] A. Grüneis, G. Kresse, Y. Hinuma, and F. Oba, Phys. Rev. Lett. **112**, 096401 (2014).
[31] C. Persson, Y.-J. Zhao, S. Lany, and A. Zunger, Phys. Rev. B **72**, 035211 (2005).
[32] Y. Kumagai, F. Oba, I. Yamada, M. Azuma, and I. Tanaka, Phys. Rev. B **80**, 085120 (2009).
[33] M. Choi, F. Oba, Y. Kumagai, and I. Tanaka, Adv. Mater. **25**, 86 (2013).
[34] P. E. Blöchl, Phys. Rev. B **50**, 17953 (1994).
[35] G. Kresse and J. Hafner, Phys. Rev. B **47**, 558 (1993).
[36] G. Kresse and J. Furthmüller, Phys. Rev. B **54**, 11169 (1996).
[37] J. P. Perdew, K. Burke, and M. Ernzerhof, Phys. Rev. Lett. **77**, 3865 (1996).
[38] J. P. Perdew and A. Zunger, Phys. Rev. B **23**, 5048 (1981).
[39] S. L. Dudarev, G. A. Botton, S. Y. Savrasov, C. J. Humphreys, and A. P. Sutton, Phys. Rev. B **57**, 1505 (1998).
[40] R. Ishikawa, N. Shibata, F. Oba, T. Taniguchi, S. D. Findlay, I. Tanaka, and Y. Ikuhara, Phys. Rev. Lett. **110**, 065504 (2013).
[41] S. Baroni and R. Resta, Phys. Rev. B **33**, 7017 (1986).
[42] M. Gajdoš, K. Hummer, G. Kresse, J. Furthmüller, and F. Bechstedt, Phys. Rev. B **73**, 045112 (2006).
[43] R. W. Nunes and X. Gonze, Phys. Rev. B **63**, 155107 (2001).
[44] J. Albertsson, S. C. Abrahams, and Å. Kvick, Acta Crystallogr. B **45**, 34 (1989).
[45] N. Ashkenov, B. N. Mbenkum, C. Bundesmann, V. Riede, M. Lorenz, D. Spemann, E. M. Kaidashev, A. Kasic, M. Schubert, M. Grundmann *et al.*, J. Appl. Phys. **93**, 126 (2003).
[46] D. Taylor, Trans. J. Br. Ceram. Soc. **83**, 5 (1984).
[47] R. E. Newnham and Y. M. de Haan, Z. Kristallogr. **117**, 235 (1962).
[48] M. Schubert, T. E. Tiwald, and C. M. Herzinger, Phys. Rev. B **61**, 8187 (2000).
[49] R. E. Hann, P. R. Suitch, and J. L. Pentecost, J. Am. Ceram. Soc. **68**, C-285 (1985).
[50] K. Kataoka, Y. Takahashi, N. Kijima, H. Nagai, J. Akimoto, Y. Idemoto, and K. Ohshima, Mater. Res. Bull. **44**, 168 (2009).
[51] K. Eichhorn, A. Kirfel, J. Grochowski, and P. Serda, Acta Crystallogr. B **47**, 843 (1991).
[52] M. E. Levinshtein, S. L. Rumyantsev, and M. S. Shur, *Properties of Advanced Semiconductor Materials: GaN, AIN, InN, BN, SiC, SiGe* (Wiley, New York, 2001).
[53] C. R. Hubbard, H. E. Swanson, and F. A. Mauer, J. Appl. Crystallogr. **8**, 45 (1975).
[54] A. S. Cooper, Acta Crystallogr. **15**, 578 (1962).
[55] T. Hom, W. Kiszenik, and B. Post, J. Appl. Crystallogr. **8**, 457 (1975).
[56] S. B. Zhang and J. E. Northrup, Phys. Rev. Lett. **67**, 2339 (1991).
[57] J. Lento, J.-L. Mozos, and R. M. Nieminen, J. Phys.: Condens. Matter **14**, 2637 (2002).
[58] I. Dabo, B. Kozinsky, N. E. Singh-Miller, and N. Marzari, Phys. Rev. B **77**, 115139 (2008).
[59] K. Fuchs, Proc. R. Soc. A **151**, 585 (1935).
[60] G. Fischerauer, IEEE Trans. Ultrason., Ferroelect., Freq. Contr. **44**, 1179 (1997).
[61] G. Petretto and F. Bruneval, Phys. Rev. Appl. **1**, 024005 (2014).
[62] W. Chen and A. Pasquarello, Phys. Rev. B **88**, 115104 (2013).
[63] Y. Hinuma, F. Oba, Y. Kumagai, and I. Tanaka, Phys. Rev. B **88**, 035305 (2013).
[64] Y. Hinuma, F. Oba, Y. Kumagai, and I. Tanaka, Phys. Rev. B **86**, 245433 (2012).
[65] W. Chen, C. Tegenkamp, H. Pfnür, and T. Bredow, Phys. Rev. B **82**, 104106 (2010).
[66] F. Oba, M. Choi, A. Togo, and I. Tanaka, Sci. Tech. Adv. Mater. **12**, 034302 (2011).
[67] F. Oba, M. Choi, A. Togo, A. Seko, and I. Tanaka, J. Phys.: Condens. Matter **22**, 384211 (2010).
[68] J. Carrasco, N. Lopez, and F. Illas, Phys. Rev. Lett. **93**, 225502 (2004).

[69] C. A. Gilbert, S. D. Kenny, R. Smith, and E. Sanville, Phys. Rev. B **76**, 184103 (2007).
[70] M. Choi, A. Janotti, and C. G. Van de Walle, J. Appl. Phys. **113**, 044501 (2013).
[71] M. J. Puska, S. Pöykkö, M. Pesola, and R. M. Nieminen, Phys. Rev. B **58**, 1318 (1998).
[72] P. A. Schultz, Phys. Rev. Lett. **96**, 246401 (2006).
[73] F. Corsetti and A. A. Mostofi, Phys. Rev. B **84**, 035209 (2011).
[74] P. A. Schultz and O. A. von Lilienfeld, Modell. Simul. Mater. Sci. Eng. **17**, 084007 (2009).
[75] J. Shim, E.-K. Lee, Y. J. Lee, and R. M. Nieminen, Phys. Rev. B **71**, 035206 (2005).
[76] H. J. Monkhorst and J. D. Pack, Phys. Rev. B **13**, 5188 (1976).
[77] C. Varvenne, F. Bruneval, M.-C. Marinica, and E. Clouet, Phys. Rev. B **88**, 134102 (2013).
[78] K. Momma and F. Izumi, J. Appl. Crystallogr. **41**, 653 (2008).